https://doi.org/10.5194/essd-2026-934
Preprint. Discussion started: 27 November 2026
© Author(s) 2026. CC BY 4.0 License.



Open Access Earth System Science Data Discussions

Global network of virtual coastal stations from altimetry-based sea level data

Lancelot Leclercq[1], Anny Cazenave[1], Fabien Léger[1], Florence Birol[1], Marcello Passaro[2], Fernando Niño[1], Léna Tolu[1], Jean-François Legeais[3], Svetlana Jevrejeva[4] and Sarah Connors[5]

1. Université de Toulouse, LEGOS (CNES/CNRS/IRD/UT3), 31401 Toulouse, Cedex 9, France
2. Deutsches Geodätisches Forschungsinstitut der Technischen Universität München, 80333 Munich, Germany
3. Collecte Localisation Satellites, Ramonville Saint-Agne, France
4. National Oceanography Center, L3 5DA, Liverpool, UK
5. European Space Agency, Climate Office, Oxfordshire OX11 0F, UK

Submitted version

Earth System Science Data (ESSD)

13 November 2026

Corresponding authors: A. Cazenave (anny.cazenave@utoulouse.fr) and L. Leclercq (lancelot.leclercq@utoulouse.fr)

https://doi.org/10.5194/essd-2026-934
Preprint. Discussion started: 27 November 2026
© Author(s) 2026. CC BY 4.0 License.



Abstract

Classical radar altimetry performs poorly in coastal areas because land reflections in the radar echoes interfere with the ocean signal, leading to spurious radar waveforms close to the coast. In recent years, dedicated reprocessing efforts have been deployed to retrieve valid sea surface height data in the world's coastal zones. Here we present the results of such a reprocessing. It has been implemented in the context of the Climate Change Initiative program of the European Space Agency and consists of retracking the raw radar waveforms (with ALES, an algorithm adapted to coastal zones) of the Jason-1, 2, 3 and Sentinel-6A Michael Freilich missions over January 2002 to December 2024, and improving the geophysical corrections applied to the altimetry data. This reprocessing, applied to high-resolution (20 Hz) along-track data, allows us to provide at each 20 Hz point, sea level time series within a band 20 km wide along the coasts, with a quasi worldwide coverage. Sea level trends are also estimated. The closest point to the coast is called ‘virtual station’. A new network of 1653 virtual stations is thus proposed, located at a mean distance of ~4 km from the coast, with 20% of them closer than 2 km. The averaged coastal sea level trend at the 1653 virtual stations, amounting 3.45 +/- 1.6 mm/yr, is not significantly different from the global mean sea level rise over the study period (equal to 3.85 +/- 0.3 mm/yr), considering associated uncertainties. However, some regions like the Gulf of Mexico, southeast US coast and west coast of India display sea level trends larger than the global mean. Similarly, the mean coastal acceleration is not significantly different from the global mean acceleration over the study time span. The coastal sea level time series are compared to other altimetry data sets, in terms of correlation and RMSE differences. Comparisons with tide gauge records at sites located at less than 60 km from a virtual station are also shown for detrended time series, with general good consistency. Finally, the use of good quality vertical land motions derived from GNSS (Global Navigation Satellite System) solutions at sites nearby tide gauges, allow us to provide relative sea level trends at a subnetwork of virtual coastal stations.

https://doi.org/10.5194/essd-2026-934
Preprint. Discussion started: 27 November 2026
© Author(s) 2026. CC BY 4.0 License.



1. Introduction

Although still modest, the current rise in sea level has already significant effects on low-lying coastal regions, particularly during extreme events (storms, cyclones) and high-amplitude tides (IPCC, 2019, 2021). It is clear that a potential sea-level rise several times greater than today's by the end of this century will have major negative impacts on many coastal regions around the world. Monitoring sea level change in the world's coastal zones is thus a major objective for at least two reasons: (1) developing adaptation strategies in regions already impacted by present-day sea level rise, and (2) offering constraints on climate models simulating future coastal sea level changes.

Two main tools are currently used to measure sea level: in situ tide gauges and satellite altimetry. Tide gauges measure sea level variations with respect to the coast. This measurement is called 'relative' sea level. Satellite altimetry measures the height of the sea surface expressed in a geocentric reference frame (called 'absolute' sea level). Absolute sea level variations result from changes in the volume of water filling ocean basins (either due to water density or mass changes) while relative sea level variations designate sea surface height changes with respect to the ground (accounting thus for both 'absolute' sea level changes plus vertical land motions).

In coastal areas, absolute variations in sea level result from the global mean rise and regional trends on which small-scale coastal processes are superimposed. These include changes in coastal currents, as well as changes in seawater density due to the delivery of fresh water by rivers into estuaries (Woodworth et al., 2019, Piecuch et al., 2018, Durand et al., 2019, Becker et al., 2024). Unlike altimetry-based sea level measurements in the open ocean, measurements collected in coastal areas are usually of reduced quality. Indeed, conventional nadir altimetry missions have been optimized to observe the open ocean. In a band of about 15 km around the coastline, the radar echoes reflected towards the satellite from which sea level measurements are deduced, are contaminated by reflections from land and patches of very calm water within the satellite footprint (Vignudelli et al., 2019). However, recent studies have shown that dedicated reprocessing of radar echoes from the Jason-1, 2, 3 altimetry missions in the world coastal zones have allowed retrieving valid sea level data very close to the coast (Benveniste et al., 2020, Cazenave et al., 2022, Peng et al., 2025). This consists of applying a dedicated model (a method called 'retracking') to extract from the complex coastal radar echoes an optimized range measurement (i.e., the distance between the satellite and the instantaneous sea surface). Such approaches have been performed so far along the satellite tracks with a spatial resolution of about 350 m. In the studies mentioned above, the data points closest to the coast are used to define a specific global dataset of "virtual stations", at which long time-series of sea level data are provided along the world coastlines.

https://doi.org/10.5194/essd-2026-934
Preprint. Discussion started: 27 November 2026
© Author(s) 2026. CC BY 4.0 License.



At the date of writing, two such global data sets derived from altimetry have been produced:

(1) the coastal sea level product called IAS2024 (Peng et al., 2025) uses the data from the Jason-1, 2 and 3 altimetry missions and combines different retrackers to estimate the altimeter range, depending on the characteristics of the radar waveform (Peng et al., 2023). This dataset provides along-track sea level time series from 2002 to 2022 at ~1600 virtual coastal stations. It is publicly available at https://doi.org/10.5281/zenodo.1320805.

(2) the other data set is produced in the context of the European Space Agency (ESA) Climate Change Initiative (CCI) coastal sea level project (Benveniste et al., 2020, Cazenave et al., 2022; https://climate.esa.int/en/projects/sea-level/). It uses the 'Adaptative Leading Edge Sub' waveform (ALES) retracking algorithm (Passaro et al., 2014, 2018) and improved geophysical corrections for the coastal zones (Birol et al., 2021). Several versions have been produced during the past few years, extending from one version to another the temporal and spatial coverages, improving the data processing and using updated geophysical corrections. The most recent version (called v4, November 2026) provides a 23-year long (2002-2024) monthly sea level dataset (time series and trends) at 1653 'virtual' coastal stations located within 8 km from the coast.

The purpose of this study is to present this latest data set (SL_cci, version v4). It combines the Jason 1/2/3 and Sentinel-6A Michael Frielich/MF satellites sea level measurements from January 2002 to December 2024. It provides coastal sea level time series and associated trends between 66° N and 66° S (the latitudinal coverage of the Jason and Sentinel-6A MF orbits), in places where the Jason and Sentinel-6A MF altimeter ground tracks cross the coastline. Section 2 presents the altimeter data used in this study as well as auxiliary data used for the validation (gridded sea level products from classical nadir altimetry missions, IAS 2024 coastal data from Peng et al. (2025), tide gauge sea level data, and GNSS (Global Navigation Satellite Systems)-based vertical land motions. Section 3 describes the different steps of the data processing. Results are presented in section 4. Section 5 compares the v4 results with other coastal sea level data, both in terms of interannual variability and trends. In section 6 is proposed a sub network of coastal stations where absolute CCI v4-based sea level trends are corrected for GNSS-based vertical land motions, leading to relative sea level trends. A discussion of the results is provided in section 7. Concluding remarks are provided in section 8.

2. Data

2.1 Raw altimetry data used to produce the CCI coastal sea level dataset (version v4)

https://doi.org/10.5194/essd-2026-934
Preprint. Discussion started: 27 November 2026
© Author(s) 2026. CC BY 4.0 License.



High-resolution (20 Hz) along-track data from the Geophysical Data Record products (GDRs) of the Jason-1 (January 2002 to January 2009), Jason-2 (February 2009 to September 2016), Jason-3 (October 2016 to June 2021) and Sentinel-6A MF (July 2021 to December 2024) altimetry missions have been considered. This continuous record thus covers the period January 2002 to December 2024. The most up-to-date versions of the GDR files have been considered : GDR-E for Jason-1, GDR-D for Jason-2 and GDR-F for Jason-3 (www.aviso.altimetry.fr). Sentinel-6A MF level 2 data are distributed by Eumetsat (www.eumetsat.int).

2.2 Gridded altimetry products

We used the monthly mean 0.25°×0.25° gridded altimetry-based sea level anomaly (SLA) data, version DT2024, downloaded from the Copernicus Climate Change Service (C3S) (Copernicus Climate Change Service, Climate Data Store, 2018) and based on the 2024 version of Level-2P input data (Kocha et al., 2026). The data set is based on a steady two-satellite merged constellation at all time steps: one satellite ensures the long-term stability of the data record (i.e., Topex/Poseidon/Jason series, Sentinel-6A MF) and the other satellite is used to improve accuracy, sample mesoscale processes and provide coverage at high latitudes. The DT2024 data set is not corrected for the absolute Glacial Isostatic Adjustment (GIA) effect. Hence, in this work, we further applied the absolute GIA correction of the ICE6G-D model from Peltier et al. (2018) to the C3S gridded SLAs. This data set is used over the January 2002 to December 2024 time span.

2.3 IAS 2024 coastal sea level product

This high-resolution along-track sea level dataset has been produced by the International Altimetry Service (IAS) team (International Altimetry Service, 2024 ; Peng et al., 2025). Only Jason-1, Jason-2 and Jason-3 missions are considered, covering the January 2002 to April 2022 time span. The data consist of 1548 virtual stations but for the comparison with the SL_cci v4 data, only the common 1122 virtual stations are considered.

2.4 Tide gauge data

Monthly values of tide gauges records from the Permanent Service for Mean Sea Level (PSMSL, https://www.psmsl.org, Holgate et al., 2013) are used. Only tide gauge records with at least 80 % of valid data over the January-2002-December 2024 time span are considered. To be consistent with altimetry data, tide gauges data are corrected for atmospheric loading, using the same correction applied to altimetry data (see section 3.3). Finally, outlier removal is performed by

https://doi.org/10.5194/essd-2026-934
Preprint. Discussion started: 27 November 2026
© Author(s) 2026. CC BY 4.0 License.



suppressing values outside the 3 times z-score envelope where $z = \frac{x-\mu}{\sigma}$, is the z-score, x the series values, μ the mean of the series and σ the standard deviation of the series.

Monthly averages are computed for all sea level data sets. In the case of the SL_cci v4 and IAS products, this means that the monthly averages of the original 10-day data are based on at most 4 orbital cycles. The seasonal (annual and semi annual) cycles are further removed by simple least-squares fit of 6- and 12-month sinusoids to the altimetry and tide gauge data.

2.5 GNSS vertical land motions (VLMs)

For the GNSS-based vertical land motions (VLMs), we use data available from the Système d'Observation du Niveau des Eaux Littorales (SONEL) database (https://www.sonel.org/-GPS-.html?lang=en). GNSS solutions from four processing centers are provided : University of La Rochelle (ULR), Nevada Geodetic Laboratory (NGL), Jet Propulsion Laboratory (JPL) and the German Research Centre for Geosciences (GFZ). For this study, we only consider the ULR20 and NGL20 solutions because at the time of this study, only these solutions are expressed in the ITRF (International Terrestrial Reference Frame) 2020 reference frame (Altamimi et al., 2023, Santamaría-Gómez et al., 2025). These consist of monthly time series covering short time spans of a few years only. We selected solutions showing quasi linear variations over time in order to be able to extrapolate the VLMs over the 2002-2024 time span considered in this study.

2.6 Distance to the coast

To estimate the distance between the coast and the satellite track, the Pacific Islands Ocean Observing System (PacIOOS) data set is used in the processing (NASA OBPG and Stumpf. 2012; https://www.pacioos.hawaii.edu/metadata/dist2coast_1deg.html). Its resolution is 0.01°.

3. Data processing

In this section, we describe the different phases of the data processing of the SL_cci coastal altimetry data (version v4). Figure 1 shows the coastal regions over which the initial data processing has been performed. These consist of 20 regions, of varying size, located around the continental coasts and tropical islands. In each region, all satellite tracks are selected for further data processing.

https://doi.org/10.5194/essd-2026-934
Preprint. Discussion started: 27 November 2026
© Author(s) 2026. CC BY 4.0 License.

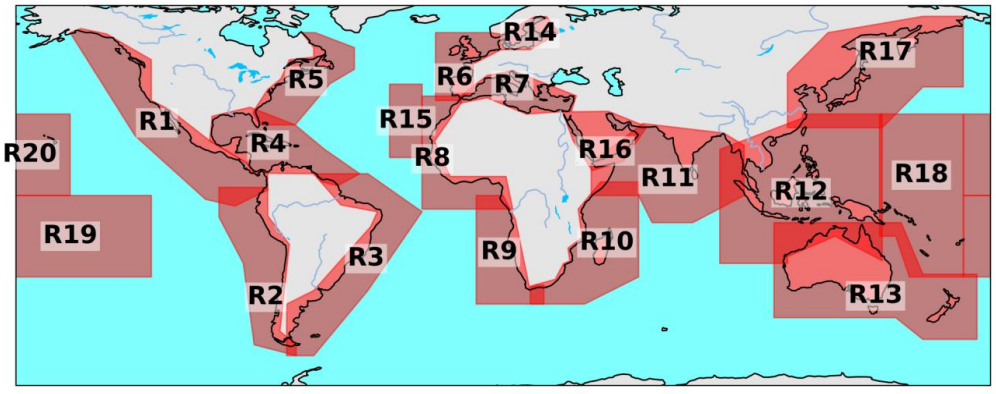


Figure 1: Location of the 20 regions (red shaded areas) considered for the SL_cci coastal altimetry data processing (version v4).

3.1 Adaptive Leading-Edge Subwaveform (ALES) retracking

This retracker was developed to increase the quality and availability of altimetry range measurements in coastal zones while maintaining open-ocean performance (Passaro et al., 2014, 2018). ALES adaptively adjusts the width of the waveform-fitting window to minimize contamination from spurious reflections. The window width is determined from an initial estimate of significant wave height, allowing ALES to retain the noise performance of full-waveform retrackers. Using the Brown–Hayne model, the algorithm also retrieves significant wave height and the backscatter coefficient, enabling the computation of a dedicated sea state bias correction. ALES retrievals have been extensively validated and applied to oceanographic studies for a wide range of applications, including coastal sea-level trends (e.g. Passaro et al., 2021), coastal sea level interannual variability (e.g., Oelsmann et al., 2024), and tidal modelling (Hart-Davis et al., 2021).

3.2 The X-TRACK system

Starting from Level-2 altimetry data, the X-TRACK production system computes Level 3 along-track SLA products with a specific editing and post-processing strategy which has the objective of retrieving as much as possible meaningful coastal altimetry measurements (Birol et al., 2017, 2021). A two-step editing strategy is used. The first step consists in rejecting potential outliers through the analysis of the different geophysical corrections. In a second step, all the correction values are interpolated from the edited data (see Birol et al., 2017, 2021 for details). The X-TRACK system is used to compute the X-TRACK products (Birol et al., 2017) which are widely used in coastal altimetry studies (Cancet et al., 2026).

https://doi.org/10.5194/essd-2026-934
Preprint. Discussion started: 27 November 2026
© Author(s) 2026. CC BY 4.0 License.



3.3 Geophysical corrections applied to the coastal sea surface height (SSH) data

Below are listed the geophysical corrections used in the X-Track processing system for the present study.

Ionospheric correction

The ionosphere correction is based on the dual-frequency altimeter range measurements, further filtered by X-TRACK (Birol et al., 2017).

Ocean tide correction

The latest FES 2022 (version b) ocean tide model (Lyard et al., 2026) is used. Compared to the previous FES 2014 ocean tide model, this new solution shows significant improvement, in particular in coastal regions. It is based on the GEBCO 2020 bathymetric database (https://www.gebco.net/data-products/gridded-bathymetry-data/gebco-2020/), combined with local and regional bathymetric data, and updated coastline products. More details can be found in Lyard et al. (2026).

Wet tropospheric correction

For the Jason-1, Jason-2 and Jason-3 missions, we use the GPD+ wet tropospheric correction (Fernandez, 2015). The GPD+ algorithms estimates the wet-tropospheric delay in satellite radar-altimetry measurements by using valid onboard radiometer data where available, and where needed, combining nearby observations from other radiometers and GNSS stations. Additionally, it inter-calibrates data with the SSM/I (Special Sensor Microwave Imager) passive microwave radiometer datasets, known for their stability. Note that because the GPD+ wet tropospheric correction is not yet available for Sentinel-6A MF, we used the atmospheric wet path delay derived from the on-board microwave radiometer.

In Table 1 are summarized the geophysical corrections applied here to the SL_cci coastal SSH data.

Table 1: Geophysical corrections applied to the CCI coastal SSH data

Parameters	Source	Jason 1	Jason 2	Jason 3	Sentinel 6A
L2 standards	GDR	GDR-E	GDR-D	GDR-F	F08 (cycle 1 to 122)

https://doi.org/10.5194/essd-2026-934
Preprint. Discussion started: 27 November 2026
© Author(s) 2026. CC BY 4.0 License.



					F09 from cycle 123
Range	ALES	20 Hz Ku band ALES corrected altimeter range (Passaro et al., 2014)			
Ionospheric correction	GDR	From dual-frequency altimeter range measurements, further filtered by X-TRACK			
Dry atmospheric correction	GDR	From ECMWF (European Centre for Medium-Range Weather Forecasts) operational model			
Wet tropospheric correction	GPD+/GDR	GPD+ radiometer correction (Fernandes et al., 2015)			From the onboard radiometer
Sea surface bias (SSB)	ALES	Sea state bias correction in Ku band, ALES retracking (Passaro et al., 2018)			
Solid Earth tide	RADS	From tide potential model (Cartwright and Edden, 1973; Cartwright and Tayler, 1971)			
Pole tide	GDR	From Wahr (1985)		From Desai et al. (2015)	
Tidal Loading	CNES	From FES 2022 (Lyard et al., 2026)			
Dynamic atmospheric correction (DAC)	RADS	From MOG2D-G high frequencies (Carrere and Lyard, 2003) + inverse barometer			
Ocean tide	CNES	From FES 2022 (Lyard et al., 2026) including ocean tide, long period equilibrium tide, S1 tide			

3.4 Intermission biases

https://doi.org/10.5194/essd-2026-934
Preprint. Discussion started: 27 November 2026
© Author(s) 2026. CC BY 4.0 License.


The procedure applied to compute the intermission biases between two successive missions follows different steps :

(1) In each of the 20 coastal regions, we compute the along-track SSH differences from two successive missions during their tandem phase, and then filter and remove outliers. At this step, we get an along-track bias for each region.

(2) The along-track SSH differences from step 1 are further averaged onto a 4° x 4 ° grid considering the 20 regions all together. The corresponding gridded bias is further spatially smoothed to obtain the final intermission bias value used to compute the multi-mission SSHs. This approach ensures a smooth transition of the intermission bias between neighboring regions.

3.5 Computation of regional sea level anomalies (SLAs) and trends

Using the along-track SSHs of all successive orbital cycles, we compute an average reference ground track. Along-track data at each 20 Hz point of the successive cycles are projected onto this reference track. Because of this projection, the location of each point changes, so the resulting SSH is corrected by the difference in geoid height of these locations. We can then compute a mean sea surface at each reference point. The SSH data are then converted into SLAs by subtracting the corresponding mean sea surface. More details on the mean sea surface computation can be found in the X-TRACK/ALES Algorithm Theoretical Basis Document (https://climate.esa.int/media/documents/SLCCI_ATBD_007_AlgorithmTheoreticalBasisDoc_v1.6_signed.pdf).

3.6 Post-processing of CCI data

A post-processing editing is further performed to remove measurements of reduced quality. This post-processing editing consists of several steps applied to the along-track 10-day SLA data.

3.6.1 Coastline detection

Detection of the point where the satellite track crosses the coast is performed through two iterations. The first iteration consists of identifying successive segments along a single satellite track presenting discontinuities larger than 0.3° in latitude (since ground tracks are mainly meridionally-oriented). The second iteration computes the distance between the satellite track and the coastline using the distance to coast variable based on NASA OBPG and Stumpf. (2012) and defines segment endpoint when the distance to coast is less than 1km. It further searches for the minimum distance to coast, even if there is no intersection with the coastline.

https://doi.org/10.5194/essd-2026-934
Preprint. Discussion started: 27 November 2026
© Author(s) 2026. CC BY 4.0 License.



3.6.2 Defining valid data at each along-track 20 Hz point for each satellite mission and editing of point by point SLA time series over the whole 2002-2024 time span

This editing phase consists of defining a threshold of valid data at each 20 Hz along-track point, for each satellite mission. A value of 50% valid data over the mission duration is considered. Removal of outliers is further carried out on the basis of the 3 times z-score envelope, as described for tide gauges in section 2.4. The corresponding 10-day valid SLA data are then resampled at monthly intervals. A new outlier removal is performed on these monthly SLA time series, based on a running mean and standard deviation over 12 months. The envelope is defined as the rolling mean ± 3 times the rolling standard deviation. Out of this envelope, the data are deleted. This approach allows us to remove isolated spurious data while retaining continuous SLA extreme fluctuations.

3.6.3 Along-track editing for trend computation : removal of spurious along-track 20 Hz points

After the point by point SLA time series editing, here we remove along-track points whose time series have a standard deviation 1.5 times larger than the average of the standard deviations of a given track segment (a value of 20 km is considered). We further check whether this editing does not lead to large data gaps along the satellite track segment. Since a 20 km-long segment should contain a maximum of sixty 20 Hz points, we constrain to 30 the minimum number of valid points for each segment.

Figure 2 illustrates the different steps of the along-track editing, to avoid isolated along-track points.

Close to the coast, along-track points are removed if there is at least one missing point within the first four points (Figure 2a). If there are more than four missing points among the first thirty points, then we remove points between the coast and the gap (Figure 2b). Finally we remove points between the gap and the open sea if there are more than four missing points in the last part of the along-track segment (after the thirtieth point).

https://doi.org/10.5194/essd-2026-934
Preprint. Discussion started: 27 November 2026
© Author(s) 2026. CC BY 4.0 License.



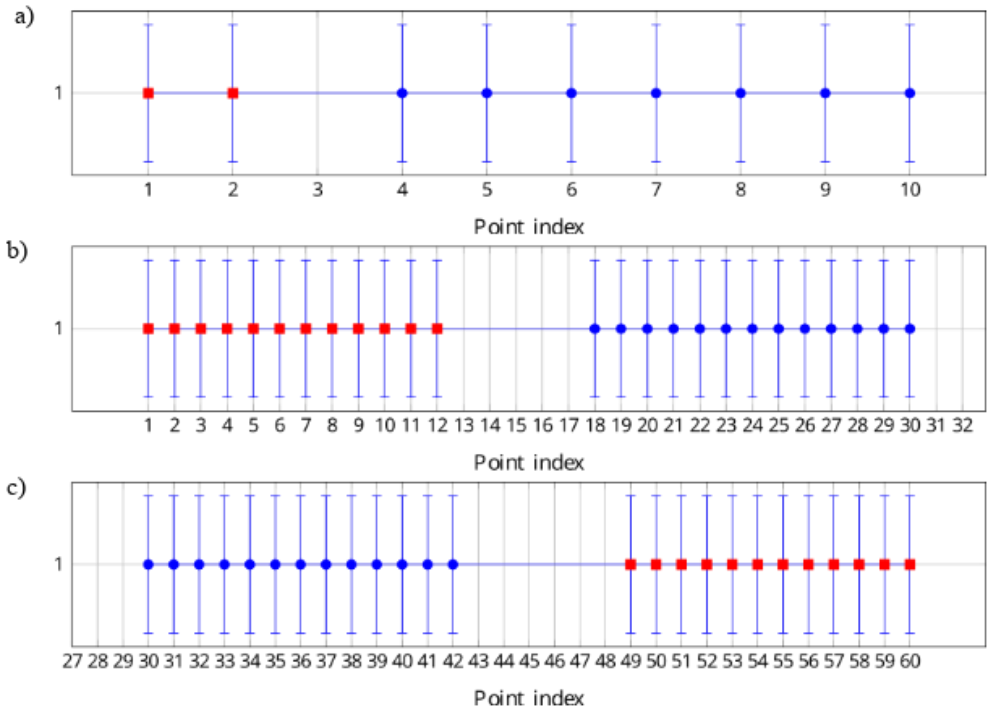


Figure 2: a) First iteration: removal of isolated points near the coast. The first two points are removed due to the missing third point among the first four points. b) Second iteration: points 1 to 12 are removed due to five missing points before the thirtieth point. c) Third iteration: points 49 to 60 are removed due to the six missing points after the thirtieth point.

3.6.4 SLA trend estimates over 2002-2024

The last step of the post-processing consists of computing SLA trends and associated trend errors using a simple least-squares fit of the SLA time series at each 20 Hz along-track point. The computed trends are further edited to remove spurious values. Outlier detection is performed using the same approach as in the second step outlier detection based on rolling mean and standard deviation as described in section 3.6.2. This is done using 2 times rolling standard deviation as an envelope. Trend errors based on the least-squares fit are likely too optimistic. More realistic trend errors accounting for errors of the geophysical corrections will be discussed in the Discussion section.

https://doi.org/10.5194/essd-2026-934
Preprint. Discussion started: 27 November 2026
© Author(s) 2026. CC BY 4.0 License.



4. Results: a new network of virtual stations and associated statistics

The data processing described above allows us to define a network of 1653 virtual stations where coastal SLA time series and associated sea level trends are provided over the January 2002 to December 2024 time span. Figure 3 shows the distribution of the 1653 coastal virtual stations along the world coastlines. Associated colors represent the distance of the first along-track valid point, i.e., defined as the distance to the coast of the virtual station.

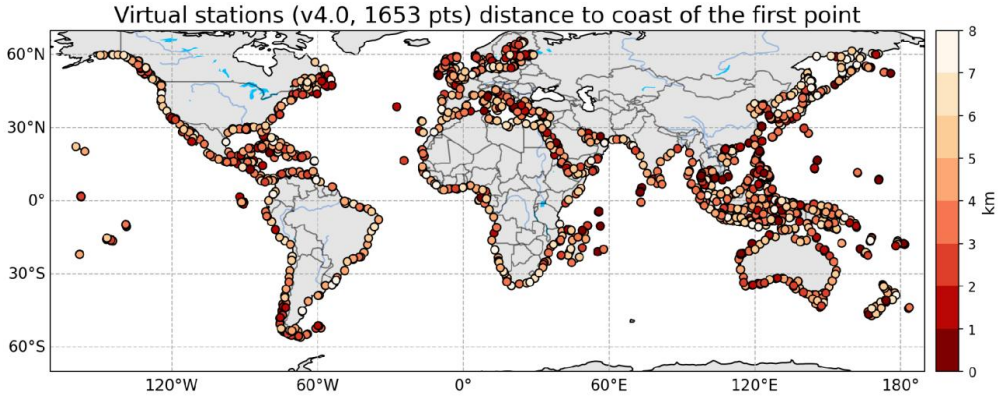


Figure 3: Distribution of the 1653 coastal virtual stations along the world coastlines. The colorbar indicates the distance (in km) of the first along-track valid point to the nearest coastline.

The mean distance value to the coast of these 1653 virtual stations is 3.9 km (see histogram in Figure 4). Trends and trend errors (from the least-squares fit) are averaged over 2 km from the closest first points to the coast. Figure 4 shows that the averaged trend of the whole dataset amounts to 3.4 mm/yr over the 2002-2024 time span, and the associated standard deviation is 1.39 mm/yr. The mean trend error based on the least-squares fit amounts to 0.7 mm/yr but as mentioned above, a more realistic trend error is twice as this, as discussed in the Discussion section.

https://doi.org/10.5194/essd-2026-934
Preprint. Discussion started: 27 November 2026
© Author(s) 2026. CC BY 4.0 License.



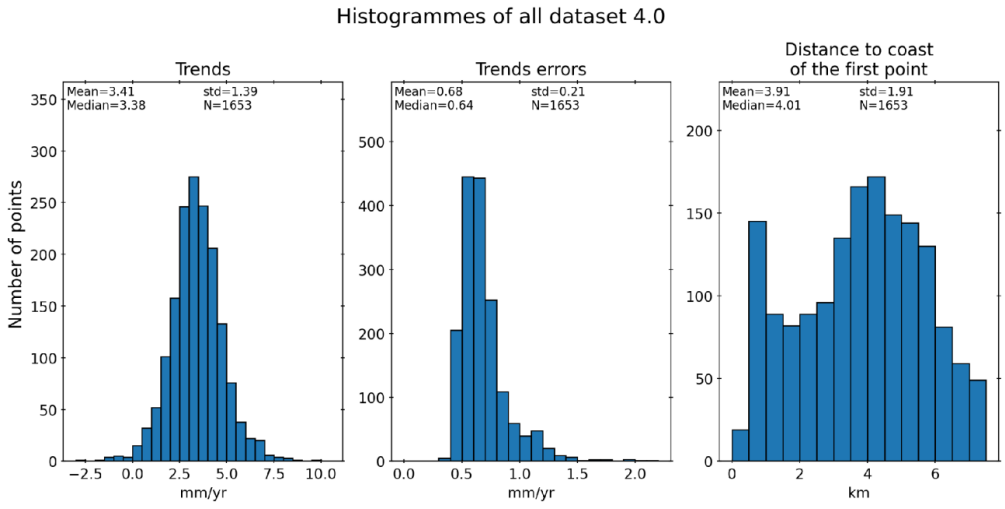


Figure 4: Histograms of the trends (left panel), trend errors (from the least-squares fit; middle panel) and distance of the closest along-track point to the coast (right panel). Trends and trend errors (in mm/yr) are averaged over 2 km from the closest first points to the coast. Distances are in km.

5. Validation

In this section the SL_cci v4 solution is compared both in terms of time series and trends with different products: the gridded C3S DT2024 data, the IAS dataset and tide gauge records. Two approaches are performed: (1) the DT2024 and IAS data are compared with the SL_cci v4 product using the SL_cci v4 virtual stations positions as reference, and (2) SL_cci v4, DT 2024 and IAS data are compared to tide gauge records at tide gauge sites colocated with the SL_cci v4 virtual stations (within 60 km). For the interannual time scale comparison, all time series are linearly detrended.

5.1 Comparison between the SL_cci (version v4) SLAs with the C3S DT2024 and IAS data sets

For this comparison, the DT2024 grids are interpolated over each SL_cci v4 virtual station track; we retain 1403 sites where both gridded data and CCI along-track data are available. We also select IAS virtual stations colocated with the SL_cci v4 virtual stations and, in this case, only IAS product along-track points common with those of the SL_cci virtual station are considered. In the end, there are 1122 common sites for the comparison between IAS and SL_cci v4 products.

https://doi.org/10.5194/essd-2026-934
Preprint. Discussion started: 27 November 2026
© Author(s) 2026. CC BY 4.0 License.

5.1.1 Detrended time series

Figure 5 shows histograms (left panels) and geographical maps (right panels) of RMSE (root mean squares error) of differences between the detrended SL_cci SLAs time series over 2002-2024 and interpolated time series from the gridded product (upper panels) and along-track IAS data (lower panels). Figure 5a,b indicates that the difference time series between SL_cci v4 and DT2024 data interpolated at 1403 sites of the virtual station network have a mean of RMSE of. 39.92 mm. On the other hand, the RMSE of the SL_cci v4 minus IAS time series amounts to 69.33 mm (1122 common sites, Figure 5 c,d). In the latter case, the largest differences between the two along-track products are seen in the North Sea, Baltic Sea, Red Sea and Southeast Asian seas and north of Australia.

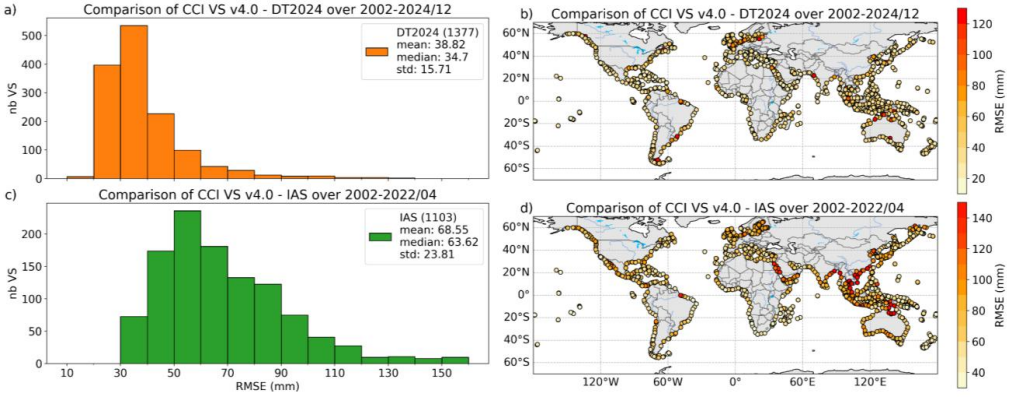


Figure 5: RMSE (mm) of the differences between SL_cci v4 data and gridded DT2024 altimetry data (a,b), and IAS data (c,d), at their common virtual station sites. Left panels : histograms. Right panels: geographical maps.

In Figure 6 are presented correlations between the detrended time series for the three data sets. Histograms (left panels) and the geographical maps (right panels) of the correlations between SL_cci v4 and DT2024 time series (Figure 6a,b) and IAS time series (Figure 6 c,d) are shown at their common virtual station sites. A slightly higher mean correlation is noted with the DT2024 gridded product than with the IAS data (0.7 versus 0.6). But although the gridded product shows the highest mean correlation, the dispersion is higher, and at some sites the correlation is very low.

https://doi.org/10.5194/essd-2026-934
Preprint. Discussion started: 27 November 2026
© Author(s) 2026. CC BY 4.0 License.

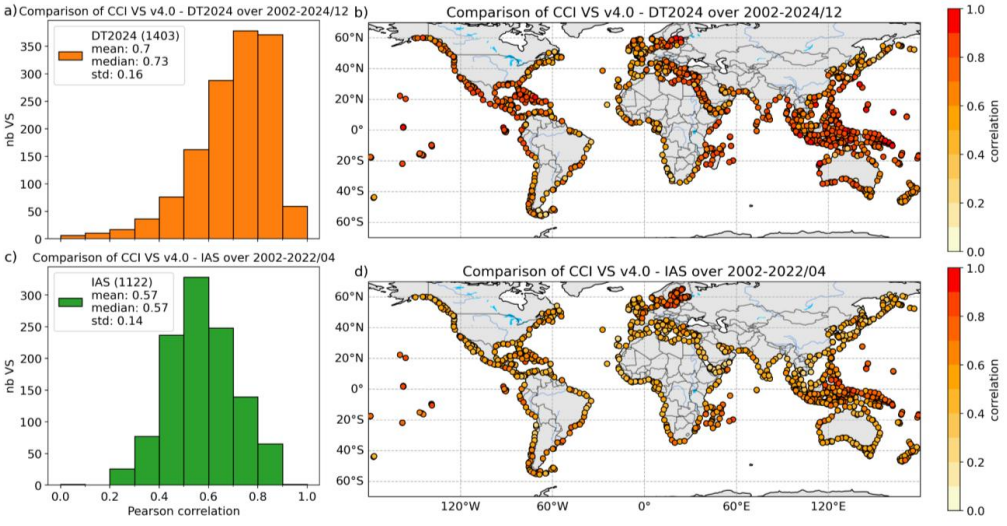
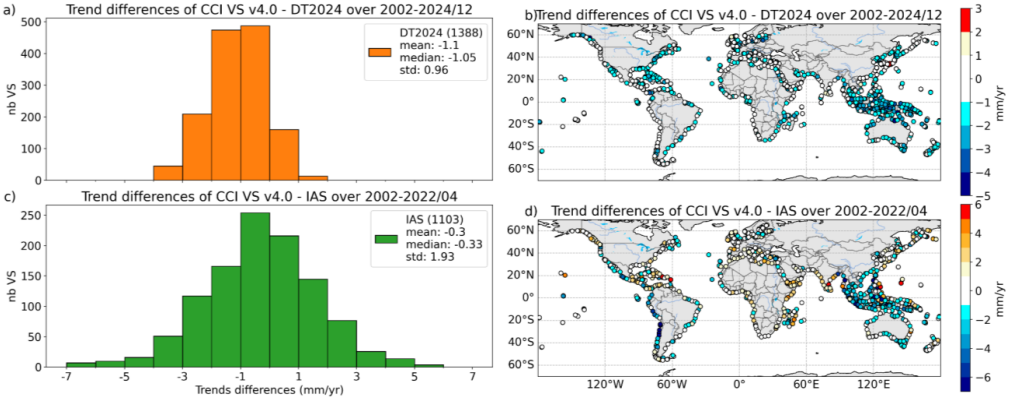


Figure 6: Correlation of the gridded DT2024 altimetry and IAS data with SL_cci v4 data at their common virtual stations. Left panels : histograms. Right panels: geographical maps.

5.1.2 Comparison of absolute trends between altimetry-based sea level data from SL_cci with products from C3S (DT2024) and IAS

Absolute trends of the SL_cci v4 product are compared with trends estimated with gridded DT2024 and IAS data. Figure 7 shows histograms of the trends differences between the datasets (Figure 7a, c) and maps of the trend differences (Figure 7b, d). Figure 7a indicates that the SL_cci v4 data and the gridded altimetry product have a small mean trend difference of -1.1 mm/yr. On the other hand, the mean trend difference with IAS data is 0.3 mm/yr, although the standard deviation is much higher, amounting 2.33 mm/yr (Figure 7c).



https://doi.org/10.5194/essd-2026-934
Preprint. Discussion started: 27 November 2026
© Author(s) 2026. CC BY 4.0 License.



Figure 7: Trend differences (mm/yr) between the gridded C3S DT2024 altimetry product, IAS product and the SL_cci v4 product. Left panels : histograms. Right panels: geographical maps.

5.2 Comparison of detrended tide gauges records with detrended SL_cci (version v4) SLAs, C3S DT2024 and IAS data (interannual time scale)

Here we compare detrended SL_cci v4, DT 2024 and IAS SLAs time series with detrended tide gauges data. Tide gauges located at less than 60 km from a SL_cci virtual station and with more than 80% of valid data over January 2002 to December 2024 are selected. The IAS virtual stations considered here are located at the same position as the SL_cci virtual stations. For the IAS dataset the time span of comparison ends in April 2022.

DT2024 grids are interpolated along the SL_cci track segment for each virtual station colocated with a tide gauge. Figure 8a,b,c shows that the C3S DT2024 product has the smallest RMSE with the tide gauge data, with an averaged value of 31.9. mm and the smallest standard deviation (16.4 mm). For the along-track products, the SL_cci v4 and the IAS products have an averaged RMSE of respectively 55.7 mm and 82.9 mm. The standard deviations of the RMSE values are respectively 23 mm and 24.5 mm.

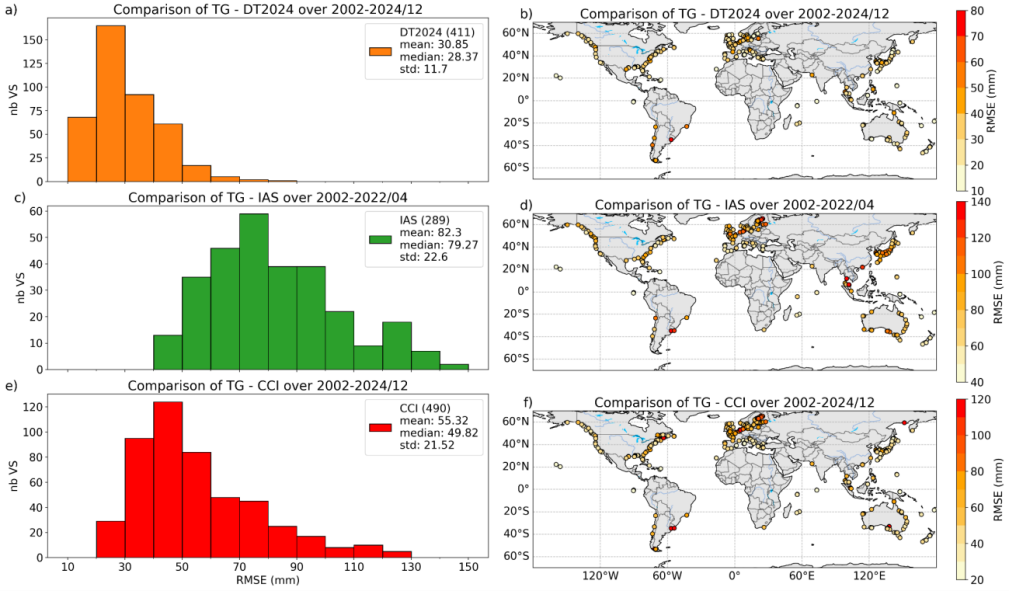


Figure 8: RMSE (mm) of the gridded DT2024 altimetry product, IAS and SL_cci v4 along-track virtual stations, compared to tide gauge records. Left panels : histograms. Right panels: geographical maps.

https://doi.org/10.5194/essd-2026-934
Preprint. Discussion started: 27 November 2026
© Author(s) 2026. CC BY 4.0 License.



Figure 9 shows the correlations between the three detrended SLA time series and detrended tide gauge records. We note that the C3S DT2024 altimetry product displays the highest correlations with the tide gauge data, with an averaged value of 0.75. For the along-track data sets, the SL_cci v4 and the IAS products have an averaged correlation with the tide gauge data of 0.58 and 0.46 respectively.

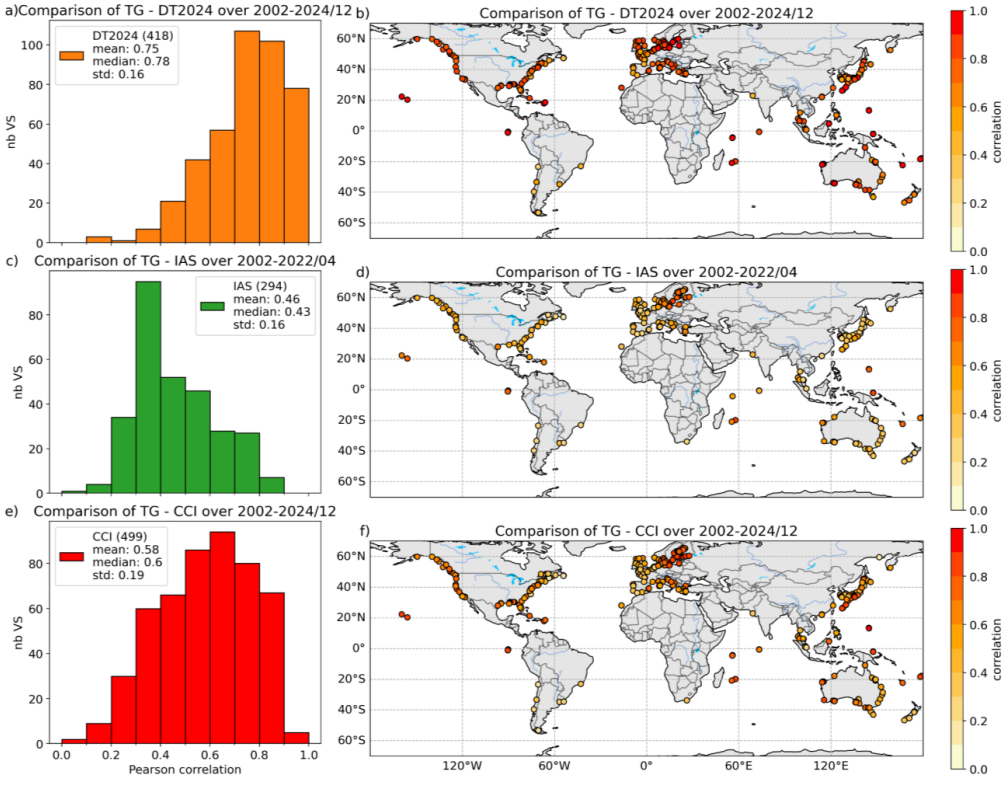


Figure 9: Correlation at their common sites between detrended gridded DT2024 altimetry product, IAS and SL_cci v4 along-track coastal virtual stations with detrended tide gauge records. Note that the number of common sites is different from one case to another. Left panels : histograms. Right panels: geographical maps.

It is worth noting that the apparent better agreement between the gridded C3S DT2024 and tide gauge data, compared to the along-track products can be explained by the different temporal sampling of the data sets: (1) monthly tide gauge data are based on averages of hourly (or higher frequency) data, (2) monthly C3S DT2024 data result from daily interpolated data, (3) the monthly SL_cci v4 and IAS averages are based on at most four orbital cycles of 10-day duration, hence at most four values for the averaging, but most of the time only two and three. Thus these monthly

https://doi.org/10.5194/essd-2026-934
Preprint. Discussion started: 27 November 2026
© Author(s) 2026. CC BY 4.0 License.



averages thus do not capture the same sea level dynamics, with the SL_cci v4 and IAS monthly data displaying more temporal variability, with a broad range of timescales (Cazenave et al., 2026a). Sea level variability along the coastline is impacted by several near-coastal processes and ocean adjustment mechanisms in shelf seas (Cipollini et al., 2018; Durand et al., 2019; Woodworth et al., 2019; Cazenave et al., 2026a), including ocean tides, local atmospheric effects or coastal trapped waves, coastal currents, and freshwater transport in estuaries. In addition, remote steric changes and open ocean mass transport contribute to the changes in near coastal sea level variability (Jevrejeva et al., 2024; Wise et al., 2024; Leclercq et al. 2025; Cazenave et al., 2026a).

5.3 Use of SL_cci SLA time series to complete nearby tide gauge records with numerous data gaps

Here we show that the SL_cci v4 SLA time series can be used to complete tide gauge records that display many data gaps. To perform the completion of the tide gauge time series, we consider tide gauge records with at least 20% of valid data over the study period. Figure 10 shows that, among the 715 tide gauges located at less than 60 km from a virtual station, 485 have more than 80% of valid data. 230 tide gauges have more than 20% of data and less than 80%.

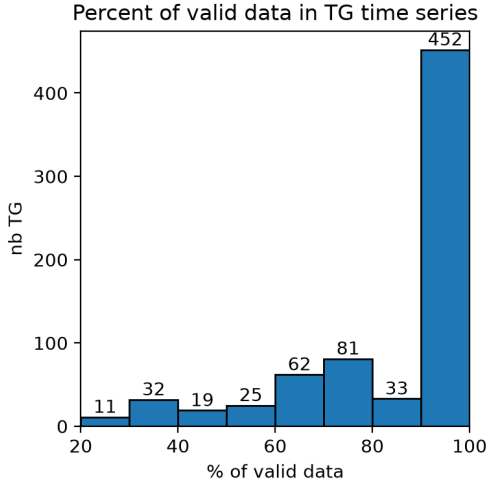


Figure 10: Histogram of the percentage of valid data in the tide gauges (TG) time series from January 2002 to December 2024.

Figure 11a,b presents two examples of tide gauge records completed with SL_cci v4 SLA time series: Kiribati Islands in the equatorial Pacific and along the coast of Denmark in the North Sea.

https://doi.org/10.5194/essd-2026-934
Preprint. Discussion started: 27 November 2026
© Author(s) 2026. CC BY 4.0 License.

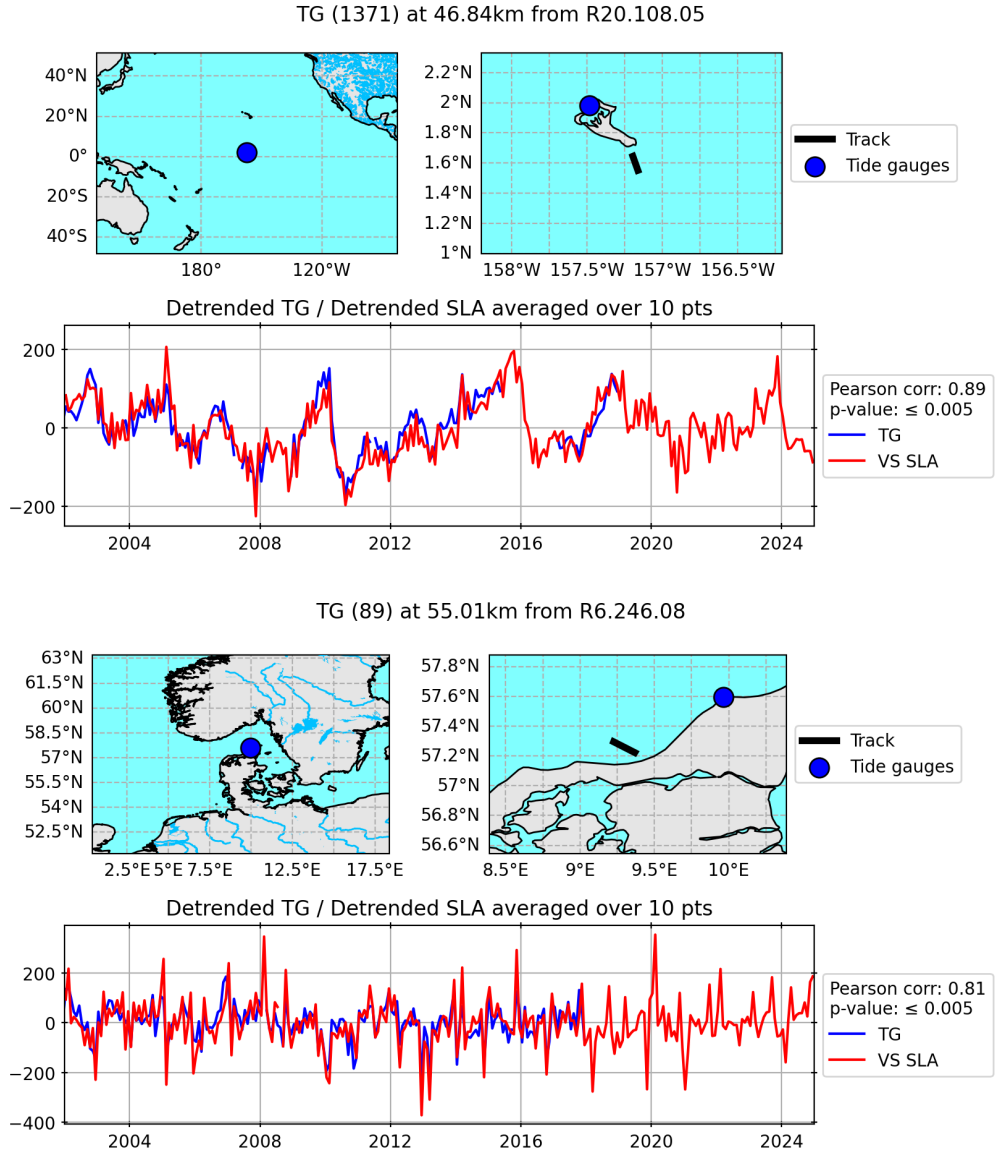


Figure 11: Detrended SL_cci SLA time series (red curve) and detrended tide gauge record (blue curve) over 2002-2024, at the Kiribati Islands, equatorial Pacific (a) and along the coast of Denmark, North Sea (b). The correlation between the two time series over their overlapping time span is indicated.

The above examples demonstrate that gaps in the tide gauge records can be filled with the coastal altimetry data with great confidence, improving the availability of sea level information for decision about adaptation strategies in regions already impacted by present-day sea level rise, in particular in low-laying small islands with limited instrumental records. Improved and extended

https://doi.org/10.5194/essd-2026-934
Preprint. Discussion started: 27 November 2026
© Author(s) 2026. CC BY 4.0 License.



tide gauge data will provide crucial information for calibration and validation numerical models, commonly used for simulation of future coastal sea level changes.

6. Relative sea level trends at the virtual stations

In this section, we estimate relative sea level trends at the virtual stations located nearby tide gauges colocated with GNSS stations. As explained in section 2, for correcting the altimetry-based sea level trends for the VLMs, here we only consider the GNSS solutions from the ULR and NGL centers, as available from the SONEL database (https://www.sonel.org).

For computing the relative sea level trends at the virtual stations and further comparing with tide gauge trends, two conditions are imposed :

(1) the tide gauge- and virtual station-based sea level time series are both almost complete (with at least 80% of data) over the 2002-2024 time span

(2) the GNSS time series display quasi linear trends, no gap, and at least 5 years of data

The second condition is based on the meticulous visual examination of the GNSS-based VLM time series. In the case of complex temporal behavior, large gaps or too short record length, the estimated VLMs are considered non reliable for correcting altimetry-based absolute sea levels.

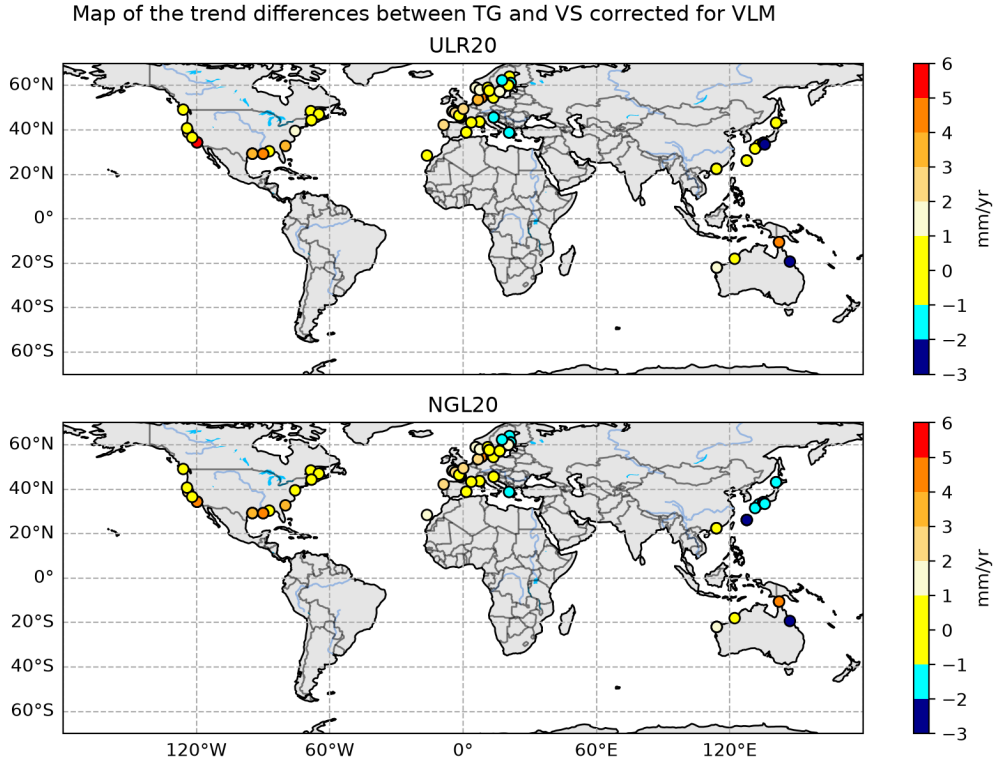
Applying the above two constraints, we have selected a list of 70 tide gauge-virtual station sites. The absolute sea level trends at the virtual stations are corrected for the VLM trends considering both the ULR and NGL GNSS trend solutions. The corresponding ‘relative’ trends are further compared to the tide gauge trends. Results are gathered in Table S1 of the Supplementary Information. They include the differences between VLM-corrected trends at the virtual stations for the two GNSS solutions, as well as tide gauge trends.

The location of the tide gauge sites colocated with a GNSS station selected for this analysis is presented in Figure 12 (with colors indicating the differences between VLM-corrected trend at the virtual stations and the tide gauge trends). Most tide gauges colocated with a GNSS station are located in the northern hemisphere. Figure 13 shows the histogram of the differences in the computed relative sea level trends for the two GNSS solutions. From figures 12 and 13, we note that most relative trend differences are within -1 and +2 mm/yr, with a peak between 0 and + 1 mm/yr.

https://doi.org/10.5194/essd-2026-934
Preprint. Discussion started: 27 November 2026
© Author(s) 2026. CC BY 4.0 License.



496



497

498 *Figure 12: Map showing the location of the tide gauge sites colocated with a GNSS station*
499 *selected for this analysis (70 sites among the 485 tide gauge sites located at less than 60 km from*
500 *a virtual station). The colored circles represent the differences in mm/yr between the tide gauge*
501 *trends and the relative trends at the virtual stations over 2002 and 2024 (SL_cci v4 absolute trends*
502 *corrected for the GNSS-based VLMs (upper panel: URL20 solution; lower panel: NGL20*
503 *solution).*

504

https://doi.org/10.5194/essd-2026-934
Preprint. Discussion started: 27 November 2026
© Author(s) 2026. CC BY 4.0 License.

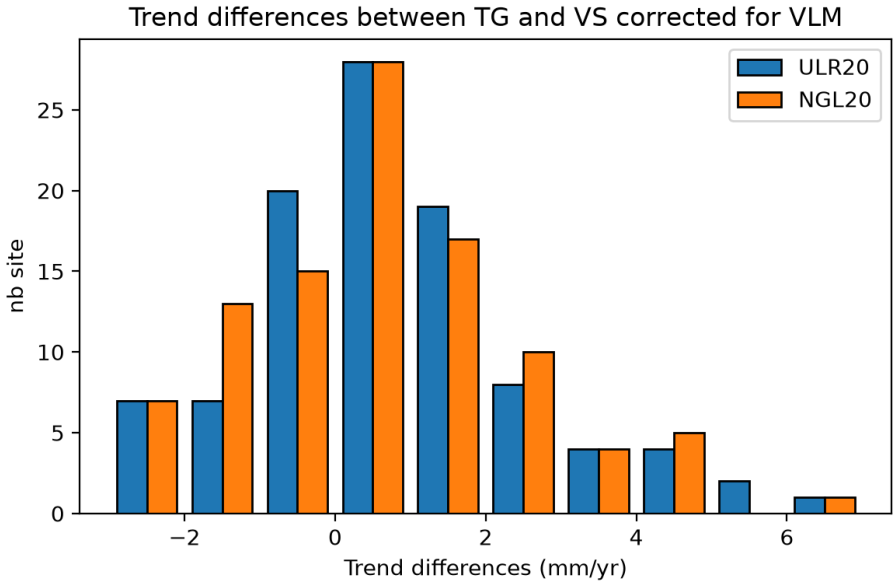


Figure 13: Histogram of the differences between VLM-corrected sea level trends at the virtual stations and TG trends estimated over 2002-2024.

7. Discussion

In this paper, we have described the latest version (v4) of the SL_cci coastal sea level product, based on the reprocessing of the Jason-1, 2, 3 and Sentinel-6A MF altimetry data in the world coastal zones. Sea level time series, 23-yr long, over January 2002 and December 2024, are provided along 1653 satellite track segments from 20 km offshore to the coast, with an along-track resolution of about 350m. A new quasi global network of 1653 virtual coastal stations located close to the coast is thus proposed. Figure 14 compares the global mean sea level curve estimated over the study time span to the coastal sea level curve based on averaging sea level data at the 1653 virtual stations. As expected, the global mean sea level curve is smoother than the latter because based on averaging many more data. The global mean trend amounts to 3.85 +/- 0.3 mm/yr while the coastal mean trend is estimated to 3.4 +/- 1.6 mm/yr. The latter uncertainty is based on realistic estimates by Tolu et al. (2026). It has been obtained by defining an error budget designed specifically for this high-resolution coastal dataset. The main error source is therefore the high frequency noise of the geophysical corrections, obtained by using the dispersion between several altimetric corrections. Associated error variance–covariance matrices are then computed for each error source, allowing to derive 90% confidence intervals for sea level trends.

https://doi.org/10.5194/essd-2026-934
Preprint. Discussion started: 27 November 2026
© Author(s) 2026. CC BY 4.0 License.



Thus considering the large uncertainty of the coastal mean sea level trend, the difference with the global mean trend is definitely not significant.

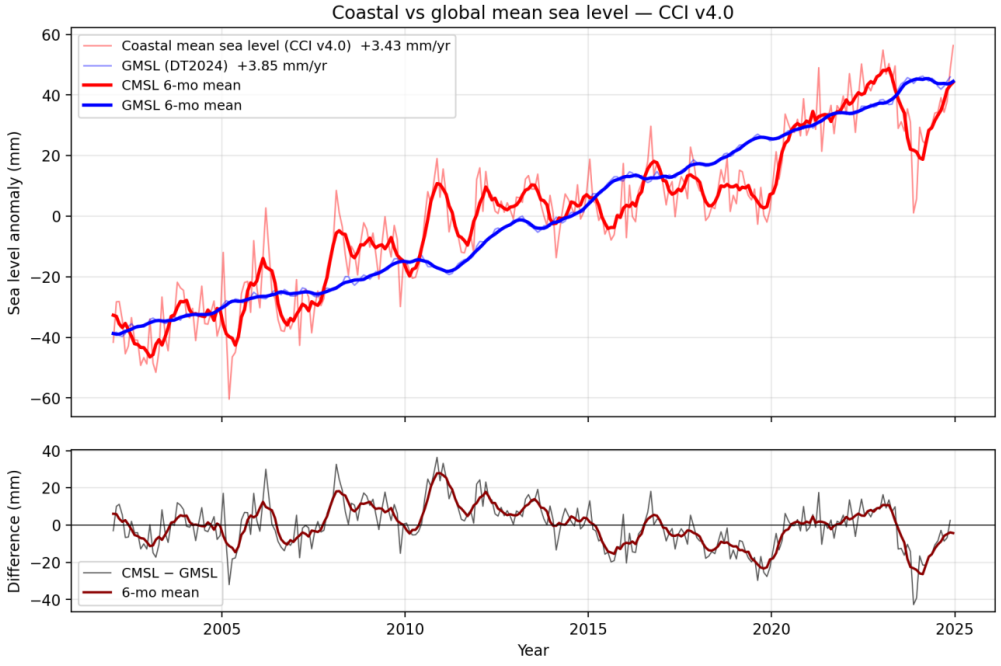


Figure 14: Upper panel: Global mean sea level (GMSL) (blue curve) and mean coastal sea level (CMSL) (red curve) over January 2002-December 2024. Lower panel: difference between CMSL and GMSL. Unit: mm. Light and thick solid curves correspond to original monthly and 6-month smoothed data respectively.

In Figure 15 is shown a map of the coastal trends at the 1653 virtual stations. We note that in many coastal regions, coastal sea level trends are similar to the global mean rise. Rates higher than the global mean are observed in the Gulf of Mexico and southeast US coast, Baltic sea, Red Sea, west coast of India, and New Zealand region. Smaller rates are noticed in the Gulf of Alaska, South America south of 40°S and South Australia.

These regional differences in coastal sea level rates are better seen when the global mean rise is removed. This is shown in Figure 16 where coastal trends corrected for the GMSL trend are displayed (only differences larger than 1 mm/yr are highlighted).

https://doi.org/10.5194/essd-2026-934
Preprint. Discussion started: 27 November 2026
© Author(s) 2026. CC BY 4.0 License.

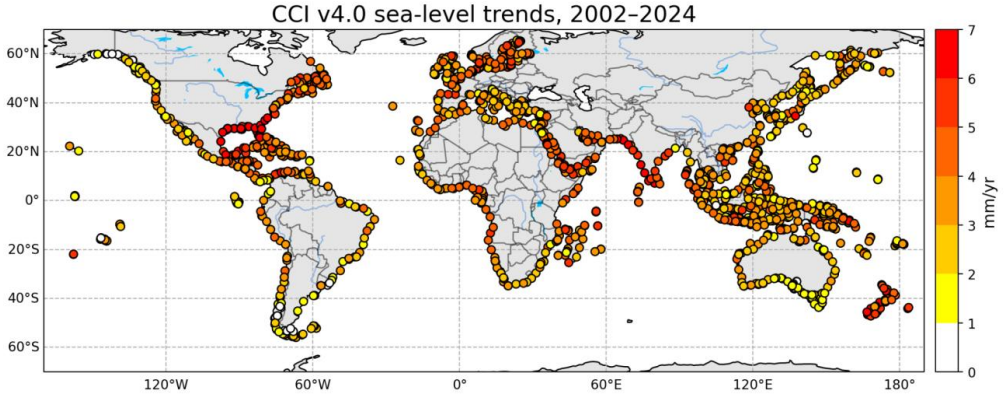


Figure 15: Coastal sea level trends (mm/yr) over January 2002-December 2024 at the 1653 virtual stations.

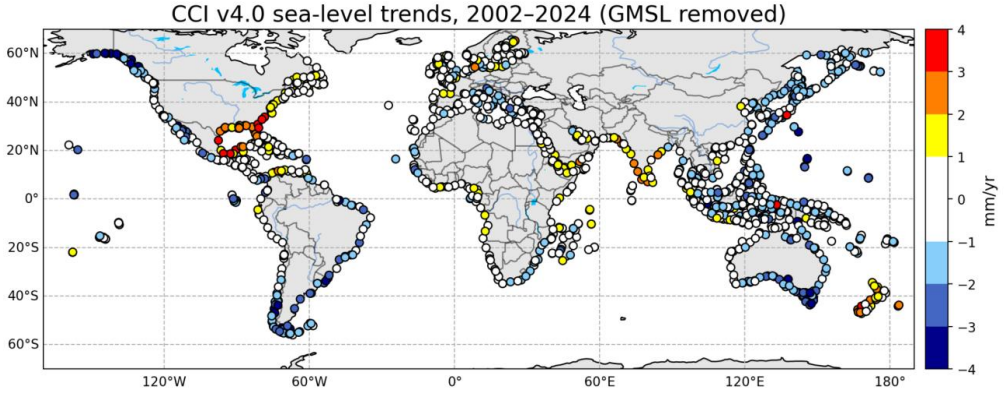


Figure 16: Differences in coastal sea level trends (mm/yr) and the global mean sea level rise over January 2002-December 2024 at the 1653 virtual stations.

Although the study time span is rather short, we also estimated the acceleration at the virtual stations over the January 2002-December 2024 time span. Results are shown in Figure 17.

https://doi.org/10.5194/essd-2026-934
Preprint. Discussion started: 27 November 2026
© Author(s) 2026. CC BY 4.0 License.

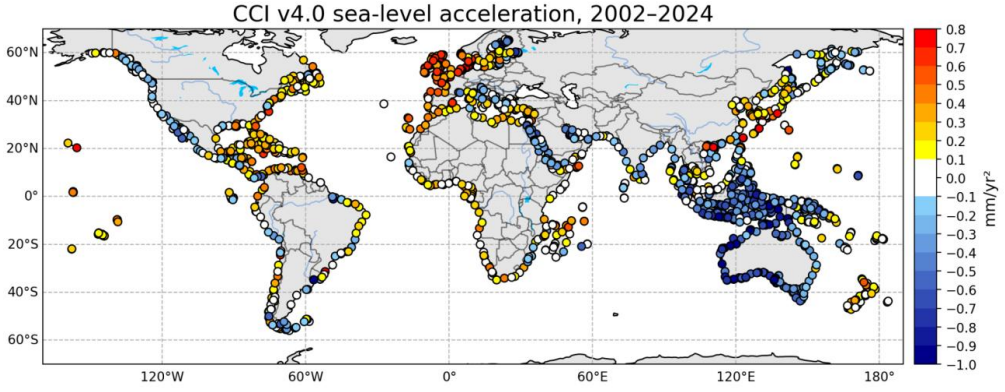


Figure 17. Acceleration (mm/yr^2) of coastal sea level over January 2002 to December 2024 at the 1653 virtual stations.

The mean coastal acceleration at the 1653 virtual stations is found to be close to zero over the January 2002 to December 2024 time span. For comparison, the global mean acceleration estimated from the DT2024 gridded data amounts to 0.1 mm/yr^2 over the same period, a value not much different from the Guerou et al's estimate for the 1993-2023 time span (equal to 0.12±0.05 mm/yr^2). As illustrated in Figure 17, strong regional variability is seen in the coastal accelerations. Some regions such as the northeast coast of America, Caribbean region, western Europe, northwest coast of Africa and northeast Asia present accelerations much higher than the 0.1 mm/yr^2 gridded global mean. This is also seen at the small tropical islands. On the other hand, the western coast of North America, Red Sea, Indian coasts, southeast Asia and Australia display accelerations smaller than the gridded global mean. Over short time spans, such as the 23-year long record considered here, regional accelerations are mostly driven by large- scale sea level variability linked to internal climate modes internal and other large-scale ocean processes (Hamlington et al., 2020; Qu et al., 2023; Steffelbauer et al., 2022). These regional accelerations thus likely reflect multidecadal climate variations rather than external forcing factors. They currently dominate the global mean sea level acceleration caused by accelerated ice sheets melting due to anthropogenic global warming (Nerem et al., 2018, Nie et al., 2026).

Recently, Qu et al. (2023) suggested that near-coastal sea level is accelerating faster than the global mean. Their study used 28 years (1993-2020) gridded satellite altimetry data (source NASA JPL, https://podaac.jpl.nasa.gov/dataset/SEA_SURFACE_Height_ALT_GRIDS_L4_2SATS_5DAY_6THDEG_V_JPL2025) covering the 80°S-80°N latitude domain, and estimated to 0.10 +/- 0.03 mm/yr^2 the sea level acceleration along the global coastline, and to 0.07 +/- 0.01 mm/yr^2 the global mean sea level acceleration. Such values slightly differ from our estimate for the mean coastal

https://doi.org/10.5194/essd-2026-934
Preprint. Discussion started: 27 November 2026
© Author(s) 2026. CC BY 4.0 License.



acceleration. However, several reasons can be invoked: (1) the time span is different (1993-2023 versus 2002-2024), (2) the record length is different (28 years versus 23 years), (3) the coverage is different (almost continuous coastline coverage over 80°S-80°N with a resolution of 0.2° in Qu et al., while our virtual stations are spaced by about 300 km at the equator and do not cover high latitudes), (4) removal of internal climate variability -ENSO (El Nino Southern Oscillation) and PDO (Pacific Decadal Oscillation) climate modes- in Qu et al., while not in our study, (5) the Topex A's instrumental drift reported over the 1993-1999 time span does not seem to be corrected for in Qu et al.'s study. Finally, use of gridded data may not fully capture the same coastal acceleration as seen at the virtual stations.

Existing uncertainties in coastal altimetry measurements (Tolu et al., 2026), together with the wide range of sea level variability affecting the relatively short sea level record from satellite altimetry (e.g., Cazenave et al., 2026a) makes difficult to precisely estimate sea level acceleration in coastal areas (Hamlington et al., 2020; Qu et al., 2023). Besides, interpreting acceleration results in coastal sea levels is challenging over short time spans, considering the lack of adequate information about the drivers of regional and local sea level rise (Hamlington et al., 2020; Qu et al., 2023, Leclercq et al., 2025). In addition, separating the wide range of variability in near coastal sea level records from satellite altimetry that result from complex interactions of various physical mechanisms along the world coastline (Hamlington et al., 2020; Cazenave et al., 2026a) is clearly a complex task. Considering all these limitations, especially the current short length of the data record, we cannot draw any definitive conclusion about any significant difference between coastal and global mean accelerations.

8. Concluding remarks

A new version of the SL_cci coastal altimeter sea level dataset (called v4) has been presented here. It differs from the previous published versions (e.g., Benveniste et al., 2020, Cazenave et al., 2022) by a spatio-temporal extension of the data (additional regions and temporal extension using the data from the Sentinel-6A MF mission), as well as by a number of improvements in the geophysical corrections and data processing. Sea level time series and estimated sea level trends over the study time span are provided at 1653 virtual coastal stations located at an averaged distance of 4 km from the coastline, sometimes at less than 1 km. Such a data set usefully completes the international tide gauge network that suffers from incomplete spatial coverage, in particular in the southern hemisphere, as well as from temporal gaps in many records.

Like tide gauge records, such an altimetry-based coastal sea level data set might be useful to decision makers in charge of developing adaptation and mitigation strategies to face the many

https://doi.org/10.5194/essd-2026-934
Preprint. Discussion started: 27 November 2026
© Author(s) 2026. CC BY 4.0 License.



environmental risks affecting coastal regions because of climate change, geohazards and human activities, especially in populated world's coastal zones. However, altimetry-based measurements only inform on absolute (climate-related) sea level change while for adaptation to sea level rise impacts, the quantity of interest is relative sea level, i.e., the combined effects of absolute sea level change and VLMs. This means that for some applications, virtual stations need to be colocated with GNSS stations, as are some tide gauge sites.

Another issue concerns the mechanisms causing coastal sea level changes. As mentioned in the introduction, coastal sea level changes result from the combination of the global mean rise, regional variations and small-scale coastal processes. The latter are in general very poorly known and may vary from one virtual station to another. To cope with this problem, high-resolution hydrodynamical models need to be developed. Although still very few are currently available, such models, once thoroughly validated with coastal altimetry observations such as those presented in this study, will contribute to improved small-scale process understanding, while filling in the spatial and temporal sparseness of the existing data (e.g., Cazenave et al., 2026a). The models may also be run in forecast mode to predict how coastal sea level will evolve in the future.

Finally, the largest limitation of the along-track coastal altimetry data set presented here is the large intertrack distance (300 km in equatorial regions), hence large along-coast gaps between successive virtual stations. Use of additional satellite altimetry missions on different orbits may improve the coastline coverage. The most promising perspective here is the use of data from the SWOT (Surface Waters Ocean Topography; Fu et al., 2024). SWOT, launched in 2022, embarks novel altimetry technology (a radar interferometer, Rodriguez et al., 2018), allowing 2 km resolution over two 50 km wide swaths on each side of the satellite track, thus providing unprecedented 2-dimensional coverage of the oceanic domain, including of the coastal zones (Morrow et al., 2019). Hence, SWOT provides much higher cross-track resolution and sea level measurements much closer to the coast than traditional nadir altimeters. SWOT observations along the coast will thus allow data continuity between adjacent satellite tracks, hence between virtual stations. Although the SWOT data record is still short, it will provide unprecedented information on the coherence (or lack of it) of along-coast sea level variations on a few years time scale, and even on longer-term changes as the SWOT record length increases.

https://doi.org/10.5194/essd-2026-934
Preprint. Discussion started: 27 November 2026
© Author(s) 2026. CC BY 4.0 License.



Data Availability

The CCI altimetry-based coastal sea level dataset (SL_cci, version v4) is distributed under CC BY 4.0 licence on the SEANOE (SEA scieNtific Open data Edition) scientific data repository in the marine sciences field. It is available at https://doi.org/10.17882/74354 (Cazenave et al., 2026b).

The raw altimetry measurements (Geophysical Data Records/GRDs) are available from AVISO (www.aviso.altimetry.fr) for the Jason-1 GDR-E, Jason-2 GDR-D and Jason-3 GDR-F. The Sentinel-6A MF level 2 GDRs are available from Eumetsat (www.eumetsat.int).

The DT2024 gridded altimetry data set is available at https://doi.org/10.24381/cds.4c328c78 (Copernicus Climate Change Service, Climate Data Store, 2018).

The IAS data are available at https://zenodo.org/doi/10.5281/zenodo.13208305 (International Altimetry Service, 2024).

Tide gauges are available from the Permanent Service for Mean Sea Level at https://www.psmsl.org (Holgate et al., 2013).

GNSS-based vertical land motions are available from the SONEL database (https://www.sonel.org/-GPS-.html?lang=en).

The global data set of distances from the nearest coastline is available from the Pacific Islands Ocean Observing System (PacIOOS) (https://www.pacioos.hawaii.edu/metadata/dist2coast_1deg.html).

Author contributions

Conceptualization: AC, JFL, FB, FL, LL, MP, FN. Methodology: FB, MP, FN, AC, JFL. Data analysis: MP, FL, LL. Data curation: LL, FL. Preparation of the figures: LL. Writing of the first version of the manuscript: AC, LL. All co-authors reviewed and edited the manuscript.

Financial support

This study is funded by the ESA Climate Change Initiative Sea Level project (https://climate.esa.int/en/projects/sea-level). LL and LT are supported by this project (grant number 4000126561/19/I-NB).

https://doi.org/10.5194/essd-2026-934
Preprint. Discussion started: 27 November 2026
© Author(s) 2026. CC BY 4.0 License.



Competing interest

The authors declare no competing interest.

Acknowledgements

The present study has benefited from previous contributions of colleagues involved in the early phases of the ESA CCI coastal sea level (SL_cci) project (F. Calafat, A. Shaw, J. Oelsmann, F. Marti, Y. Gouzenes and J. Benveniste).

References

Altamimi, Z., Rebischung, P., Collilieux, X., Métivier, L., & Chanard, K., ITRF2020: An augmented reference frame refining the modeling of nonlinear station motions. *Journal of Geodynamics*, 97(47), 47. https://doi.org/10.1007/s00190-023-01738-w, 2023.

Becker, M., Seeger, K., Paszkowski, A., Marcos, M., Papa, F., Almar, R., et al., Coastal flooding in Asian megadentals: Recent advances, persistent challenges, and call for actions amidst local and global changes. *Reviews of Geophysics*, 62, e2024RG000846. https://doi.org/10.1029/2024RG000846, 2024.

Benveniste, J., Birol, F., Calafat, F., Cazenave, A., Dieng, H., Gouzenes, Y., Legeais, J. F., Léger, F., Niño, F., Passaro, M., Schwatke, C., and Shaw, A.: Coastal sea level anomalies and associated trends from Jason satellite altimetry over 2002–2018, *Sci Data*, 7, 357, https://doi.org/10.1038/s41597-020-00694-w, 2020.

Birol F., Fuller N., Lyard F., Cancet M., Niño F., Delebecque C., Fleury S., Toublanc F., Melet A., Saraceno M. and Léger F.: Coastal applications from nadir altimetry: example of the X-TRACK regional products. *Advances in Space Research*, 59 (4), p.936-953 http://doi/org/10.1016/j.asr.2016.11.005, 2017.

Birol, F., Léger, F., Passaro, M., Cazenave, A., Niño, F., Calafat, F.M., Shaw, A., Legeais, J.-F., Gouzenes, Y., Schwatke, C., Benveniste, J., The X-TRACK/ALES multi-mission processing system: New advances in altimetry towards the coast. *Advances in Space Research* 67, 2398–2415. .https://doi.org/10.1016/j.asr.2021.01.049, 2021.

Cancet M., Birol, F., Vergara, O., Dagneaux, Q., Léger, F., Bignalet-Cazalet, F., Daguze, J.-A., Fouchet, E., Homerin, A., Maraldi, C., Niño, F., Pujol, M.-I., and Tran, N.: ALTICAP: a new global satellite altimetry product for coastal applications, *Earth Syst. Sci. Data*, 18, 2319–2347, https://doi.org/10.5194/essd-18-2319-2026, 2026.

Carrère, L., and F. Lyard Modeling the barotropic response of the global ocean to atmospheric wind and pressure forcing - comparisons with observations, *Geophys. Res. Lett.*, 30, 1275, doi:10.1029/2002GL016473, 6, 2003.

Cartwright, D. E. and Edden, A. C.: Corrected Tables of Tidal Harmonics, *Geophysical Journal International*, 33, 253–264, https://doi.org/10.1111/j.1365-246X.1973.tb03420.x, 1973.

Cartwright, D. E. and Tayler, R. J.: New Computations of the Tide-generating Potential, *Geophys J Int*, 23, 45–73, https://doi.org/10.1111/j.1365-246X.1971.tb01803.x, 1971.

https://doi.org/10.5194/essd-2026-934
Preprint. Discussion started: 27 November 2026
© Author(s) 2026. CC BY 4.0 License.



712 Cazenave, A., Gouzenes, Y., Birol, F., Leger, F., Passaro, M., Calafat, F. M., Shaw, A., Nino, F.,
713 Legeais, J. F., Oelsmann, J., Restano, M., and Benveniste, J.: Sea level along the world's coastlines
714 can be measured by a network of virtual altimetry stations, *Commun Earth Environ*, 3, 117,
715 https://doi.org/10.1038/s43247-022-00448-z, 2022.

716 Cazenave, A., Almar, R., Almeida, P. et al. Present-Day Sea Level Variations in Coastal Areas
717 from Daily to Multidecadal Time Scales: Observations and Causes. *Surv Geophys*.
718 https://doi.org/10.1007/s10712-026-09956-5, 2026a.

719 Cazenave Anny, Gouzenes Yvan, Leclercq Lancelot, Birol Florence, Legér Fabien, Passaro
720 Marcello, Calafat Francisco M, Shaw Andrew, Niño Fernando, Legeais Jean François, Oelsmann
721 Julius, Benveniste Jérôme, Connors Sarah. New network of virtual altimetry stations for measuring
722 sea level along the world coastlines. SEANOE. https://doi.org/10.17882/74354, 2026b.

723 Cipollini, P., Benveniste, J., Birol, F., Fernandes, M.J., Obligis, E., Passaro, M., Strub, P.T.,
724 Valladeau, G., Vignudelli, S., Wilkin, J., Satellite altimetry in coastal regions. In Satellite
725 Altimetry Over the Oceans and Land Surfaces; Stammer, D., Cazenave, A., Eds.; CRC Press: Boca
726 Raton, FL, USA; London, UK; New York, NY, USA; pp. 343–373, 2018.
727

728 Copernicus Climate Change Service, Climate Data Store, Sea level gridded data from satellite
729 observations for the global ocean from 1993 to present, https://doi.org/10.24381/cds.4c328c78,
730 2018.

731 Desai, S., Wahr, J., and Beckley, B., Revisiting the pole tide for and from satellite altimetry, *J*
732 *Geod*, 89, 1233–1243, https://doi.org/10.1007/s00190-015-0848-7, 2015.

733 Durand, F., Piecuch, C.G., Becker, M., Papa, F., Raju, S.V., Khan, J.U., Ponte, R.M., Impact of
734 Continental Freshwater Runoff on Coastal Sea Level. *Surv Geophys* 40, 1437–1466.
735 https://doi.org/10.1007/s10712-019-09536-w, 2019.

736 Fernandes, M. J., Lázaro, C., Ablain, M., and Pires, N., Improved wet path delays for all ESA and
737 reference altimetric missions, *Remote Sensing of Environment*, 169, 50–74,
738 https://doi.org/10.1016/j.rse.2015.07.023, 2015.

739 Fu, L.-L., Pavelsky, T., Cretaux, J.-F.,Morrow, R., Farrar, J. T., Vaze, P., et al., The Surface Water
740 and Ocean Topography Mission: A breakthrough in radar remote sensing of the ocean and
741 landsurface water. *Geophysical Research Letters*, 51, e2023GL107652.
742 https://doi.org/10.1029/2023GL107652, 2024.

743 Guérou A, Meyssignac B, Prandi P, Ablain M, Ribes A, Bignalet-Cazalet F., Current observed
744 global mean sea level rise and acceleration estimated from satellite altimetry and the associated
745 measurement uncertainty. *Ocean Sci*, 19, 431–451, https://doi.org/10. 5194/os-19- 431-2023,
746 2023.

747 International Altimetry Service: IAS2024 coastal sea level dataset,
748 https://doi.org/10.5281/ZENODO.13208305, 2024.

749 IPCC, Special Report on the Ocean and Cryosphere in a Changing Climate [H.-O. Pörtner, D.C.
750 Roberts, V. Masson-Delmotte, P. Zhai, M. Tignor, E. Poloczanska, K. Mintenbeck, A. Alegría,
751 M. Nicolai, A. Okem, J. Petzold, B. Rama, N.M. Weyer (eds.), 2019.

752 IPCC, Climate Change 2021: The Physical Science Basis. Contribution of Working Group I to the
753 Sixth Assessment Report of the Intergovernmental Panel on Climate Change [Masson-Delmotte,

https://doi.org/10.5194/essd-2026-934
Preprint. Discussion started: 27 November 2026
© Author(s) 2026. CC BY 4.0 License.



V., P. Zhai, A. Pirani, S.L. Connors, C. Péan, S. Berger, N. Caud, Y. Chen, L. Goldfarb, M.I. Gomis, M. Huang, K. Leitzell, E. Lonnoy, J.B.R. Matthews, T.K. Maycock, T. Waterfield, O. Yelekçi, R. Yu, and B. Zhou (eds.)]. Cambridge University Press, 2021.

Hamlington, B.D., Frederikse, T., Nerem, R.S., Fasullo, J.T., Adhikari, S., Investigating the acceleration of regional sea level rise during the satellite altimeter era. *Geophys. Res. Lett.*, 47, e2019GL086528, 2020.

Hart-Davis, M., Piccioni, G., Dettmering, D., Schwatke, C., Passaro, M., and Seitz, F., EOT20-A global Empirical Ocean Tide model from multi-mission satellite altimetry, Deutsches Geodätisches Forschungsinstitut, München, SEANOE, https://doi.org/10.17882/79489, 2021.

Holgate, S.J., Matthews, A., Woodworth, P.L., Rickards, L.J., Tamisiea, M.E., Bradshaw, E., Foden, P.R., Gordon, K.M., Jevrejeva, S., Pugh. New Data Systems and Products at the Permanent Service for Mean Sea Level. *Coastal Research.*, 29, 493–504. https://doi.org/10.2112/JCOASTRES-D-12-00175.1, 2013.

Jevrejeva, S., Calafat, F. M., De Dominicis, M., Hirschi, J. J. M., Mecking, J. V., Polton, J. A., Sinha, B., Wise, A., & Holt, J. Challenges, Advances and Opportunities in Regional Sea Level Projections: The Role of Ocean-Shelf Dynamics. *Earth's Future*, 12, 8, https://doi.org/10.1029/2024EF004886, 2024.

Kocha, C., Liévin, M., Pageot, Y., Rubin, C., Quet, V., Octau, F., et al., Three decades of sea level multi-mission satellite data reprocessed to improve mesoscale quality while ensuring climate scale consistency. *Earth System Science Data Discussions*, 1–40, https://doi.org/10.5194/essd-2025-604, 2026.

Leclercq, L., et al., Spatio-temporal changes in interannual sea level along the world coastlines, *Global and Planetary Change*, Volume 253, https://doi.org/10.1016/j.gloplacha.2025.104972, 2025.

Lyard, F. H., Carrère, L., Fouchet, E., Cancet, M., Ferrari, R., Dabat, M.-L., Skandrani, C., Greenberg, D., Allain, D., Dibarboure, G., and Picot, N., FES2022 global tide atlas: a step towards SWOT-compliant tidal corrections, EGUsphere [preprint], https://doi.org/10.5194/egusphere-2026-6805, 2026.

Morrow R. et al.. Global Observations of Fine-Scale Ocean Surface Topography With the Surface Water and Ocean Topography (SWOT) Mission, *Frontiers in Marine Science*, 6, 2019.

NASA Ocean Biology Processing Group (OBPG) and R.P. Stumpf, Distance to Nearest Coastline: 0.01-Degree Grid. Distributed by the Pacific Islands Ocean Observing System (PacIOOS). http://pacioos.org/metadata/dist2coast_1deg.html, 2012.

Nerem, R.S., Beckley, B.D., Fasullo, J.T., Hamlington, B.D., Masters, D., Mitchum, G.T., Climate-change driven accelerated sea-level rise detected in the altimeter era. *Proc. Natl. Acad. Sci.*, 115, 2022–2025, 2018.

Nie Y., Chen J., Slater T., Shepherd A., Otosaka I., Xiao Q. and Xu G., Greenland and Antarctica Dominate Recent Acceleration in Global Mean Sea Level Rise: 1993-2023, *Geophys. Res. Lett.*, in press., 2026.

https://doi.org/10.5194/essd-2026-934
Preprint. Discussion started: 27 November 2026
© Author(s) 2026. CC BY 4.0 License.



795 Oelsmann J., Calafat F. M., Passaro M., Hughes C., Richter K., Piecuch C., Wise A., Katsman C.,
796 Dettmering D., Seitz F., Jevrejeva, S., Coherent Modes of Global Coastal Sea Level Variability.
797 *Journal of Geophysical Research: Oceans*, 129, 12, https://doi.org/10.1029/2024jc021120, 2024.

798 Passaro, M., Cipollini, P., Vignudelli, S., Quartly, G. D., and Snaith, H. M., ALES: A multi-
799 mission adaptive subwaveform retracker for coastal and open ocean altimetry, *Remote Sensing of*
800 *Environment*, 145, 173–189, https://doi.org/10.1016/j.rse.2014.02.008, 2014.

801 Passaro, M., Nadzir, Z. A., and Quartly, G. D., Improving the precision of sea level data from
802 satellite altimetry with high-frequency and regional sea state bias corrections, *Remote Sensing of*
803 *Environment*, 218, 245–254, https://doi.org/10.1016/j.rse.2018.09.007, 2018.

804 Passaro M., Müller F.L., Oelsmann J., Rautiainen L., Dettmering D., Hart-Davis M.G.,
805 Abulaitijiang A., Andersen O.B., Høyer J., Madsen K., Ringgaard I., Särkkä J., Scarrott R.,
806 Schwatke C., Seitz F., Tuomi L., Restano M., Benveniste J., Absolute Baltic Sea Level Trends in
807 the Satellite Altimetry Era: A Revisit. *Frontiers in Marine Science*, 8,
808 https://doi.org/10.3389/fmars.2021.647607, 2021.

809 Prandi, P., Meyssignac, B., Ablain, M. et al., Local sea level trends, accelerations and uncertainties
810 over 1993–2019. *Nature Sci Data*, 626, 8, 1. https://doi.org/10.1038/s41597-020-00786-7, 2021.

811
812 Peltier, R. W., Argus, D. F., and Drummond, R.: Comment on "An assessment of the ICE-
813 6G_C(VM5a)glacial isostatic adjustment model" by Purcell et al., *J. Geophys. Res.-Solid Earth*,
814 123, 2019-2028, 2018.

815 Peng, F. K., Deng, X. L., Jiang, M. F., Dinardo, S., and Shen, Y. Z.: A new method to combine
816 coastal sea surface height estimates from multiple retrackers by using the Dijkstra algorithm,
817 *Remote Sens.*, 15, 2329, https://doi.org/10.3390/rs15092329, 2023.

818 Peng, F., Deng, X., Shen, Y., and Cheng, X., The International Altimetry Service 2024 (IAS2024)
819 coastal sea level dataset and first evaluations, *Earth System Science Data*, 17, 1441–1460,
820 https://doi.org/10.5194/essd-17-1441-2025, 2025.

821 Piecuch, C. G., Bittermann, K., Kemp, A.C., Ponte, R.M., Little, C.M., Engelhart, S.E., Lentz,
822 S.J., River-discharge effects on United States Atlantic and Gulf coast sea-level changes.
823 *Proceedings of the National Academy of Sciences*, 115, 7729–7734.
824 https://doi.org/10.1073/pnas.1805428115, 2018

825 Qu, Y., Jevrejeva, S., Palanisamy, H., Are Near-Coastal Sea Levels Accelerating Faster Than
826 Global during the Satellite Altimetry Era? *Atmosphere*, 14, 1573.
827 https://doi.org/10.3390/atmos14101573, 2023.

828 Rodriguez, E, D Esteban Fernandez, E Peral, C W Chen, J-W De Bleser, B Williams. Wide-swath
829 altimetry: A review. In: "Satellite altimetry over oceans and land surfaces", Book Chapter 2. Eds
830 D. Stammer & A. Cazenave, CRC Press, Taylor and Francis Group, Boca Raton, New York,
831 London, ISBN: 13: 978-1-4987-4345-7, 2018.

832
833 Santamaría-Gómez, A., Boy, J.-P., Feriol, F., Gravelle, M., Loyer, S., Nahmani, S., Nicolas, J.,
834 García Pallero, J. L., Panetier, A., Pollet, A., Sakic, P., and Wöppelmann, G.: Monitoring the
835 Earth's deformation with the SPOTGINS series, *Earth Syst. Sci. Data*, 17, 5833–5840,
836 https://doi.org/10.5194/essd-17-5833-2025, 2025.
837

https://doi.org/10.5194/essd-2026-934
Preprint. Discussion started: 27 November 2026
© Author(s) 2026. CC BY 4.0 License.



838 Steffelbauer et al., Evidence of regional sea-level rise acceleration for the North Sea, *Environ. Res.*
839 *Lett.*, 17 074002, https://doi.org/10.1088/1748-9326/ac753a, 2022.
840
841 Tolu et al., Quantifying uncertainties in coastal sea level trends estimates using Jason altimetry
842 observations (2002-2021), submitted, *Scientific Data*, 2026.

843 Vignudelli, S. et al., Satellite altimetry measurements of sea level in the coastal zone. *Surveys in*
844 *Geophysics*, https://doi.org/10.1007/s10712-019-09569-1, 2019.
845

846 Wahr, J. M.: Deformation induced by polar motion, *Journal of Geophysical Research: Solid Earth*,
847 90, 9363–9368, https://doi.org/10.1029/JB090iB11p09363, 1985.

848 Wise, A., Calafat, F. M., Hughes, C. W., Jevrejeva, S., Katsman, C. A., Oelsmann, J., Piecuch, C.,
849 Polton, J., & Richter, K., Using Shelf-Edge Transport Composition and Sensitivity Experiments
850 to Understand Processes Driving Sea Level on the Northwest European Shelf. *Journal of*
851 *Geophysical Research-Oceans*, 129(5). https://doi.org/10.1029/2023JC020587, 2024.

852 Woodworth, P.L. et al., Forcing Factors Affecting Sea Level Changes at the Coast. *Surveys in*
853 *Geophysics*, 40, 1351–1397, https://doi.org/10.1007/s10712-019-09531-1, 2019.
854
855
856
857